Quantitative Analysis of Aerosol Influence on Suomi-NPP VIIRS Nighttime Light in China

Xuejun Wang, Xihan Mu, and Guangjian Yan, *Senior Member, IEEE*

***Abstract*—As a primary nighttime light (NTL) data source, the day/night band (DNB) sensor of the visible infrared imaging radiometer suite (VIIRS) is used in a wide range of studies. However, this signal is influenced by the atmosphere and may cause uncertainty while monitoring ground NTL. Given the lack of the quantitative analysis of the atmospheric effect on NTL, this study analyzes the relationship between VIIRS DNB NTL radiance and aerosol optical depth (AOD) in the urban areas of Beijing and three other Chinese cities of different urbanization levels. Results suggest a significantly negative relationship between the NTL radiance and AOD. The linear and log-linear models generate similar coefficients of determination (R^2) for the AOD and NTL data, which vary for different urban centers. In Beijing, where the aerosol robotic network observations are available, R^2 reached 0.655 between the monthly NTL radiance and AOD. A slight decrease of R^2 occurred while using the Himawari AOD. The relationship between the NTL radiance and AOD varies among the cities. The NTL radiance may decrease by approximately 10 nW.cm^{-2}sr^{-1} when daily AOD increases one unit. For Beijing, this decrease may be above 15 nW.cm^{-2}sr^{-1}, which is comparable with the threshold used to extract urban areas. These findings underscore the importance of AOD in the application of NTL data that are potentially useful in the reconstruction of stable time series VIIRS DNB images by removing the aerosol effects.**

***Index Terms*—Aerosol optical depth (AOD), atmospheric effect, nighttime light (NTL), national polar-orbiting partnership visible infrared imaging radiometer suite (NPP-VIIRS), quantitative analysis.**

I. Introduction

NIGHTTIME light (NTL) remote sensing data reflect the distribution and intensity of the artificial light at night. The two main sources of NTL data are the defense meteorological satellite program–operational linescan system (DMSP OLS) and visible infrared imaging radiometer suite (VIIRS) day/night band (DNB) sensor, onboard the Suomi national polar-orbiting partnership (NPP) and joint polar satellite system satellite platforms [1]. The DMSP OLS data were no longer the primary data being processed for NTL after 2013 when the VIIRS DNB data were available. Compared with DMSP OLS, the VIIRS DNB has significant improvements in sensor resolution and calibration, which can acquire a global daily nighttime visible and near-infrared information from cities, towns, industrial sites, and other human activities [2]. These improvements allow for better monitoring of both the magnitude and signature of the nighttime phenomena. The VIIRS DNB NTL images are used in a wide range of research fields, including demographic and socioeconomic indicators [3]–[9], short-term features detection [10]–[13], settlement dynamics [14]–[18], nighttime atmospheric properties [19]–[25], short- and long-term change detection [26]–[28], and other topics, such as light pollution [29], [30] and CO_2 emissions [31], [32].

Numerous factors, including moonlight, atmosphere, snow, and clouds, affect the quality of the NTL images [33] and adversely impact the data application and analysis. Atmospheric scattering [34] and absorption [35] (especially the atmosphere with high-concentration aerosols) can considerably affect the signal detected by the satellite sensor. An aerosol optical depth (AOD) is an important parameter in measuring the degree of atmospheric extinction that can also be used as an effective substitute to track the evolution of the aerosol-induced air pollution [36]. The VIIRS DNB radiance is sensitive to the changes of aerosols and, thus, can be used as an indicator of air quality changes [23]. Johnson *et al*. [19] and McHardy *et al*. [20] presented the methods of retrieving nighttime AOD using the contrast between the adjacent VIIRS DNB pixels. Román *et al*. [37] proposed an atmospheric correction method for VIIRS DNB daily products. However, most studies and analyses do not consider aerosols when using NTL data. Limited research quantitatively explores the relationship between the aerosols and NTL radiance.

A heavily polluted atmosphere with increased AOD may produce an even greater impact on the quality of NTL images. Air pollution is increasingly becoming severe in developing countries with rapid economic growth and urbanization [38]. Air pollution in China gradually worsened since the year 2000 and has recently drawn public attention [39]. At present, the air quality in China is improving due to adopted systematic measures [40], [41]. Therefore, an analysis is important to determine the atmospheric effect and its extent on the NTL data in China.

This study aims to quantitatively investigate the relationship between the NTL radiance and AOD using the daily and monthly data in China. Four Chinese cities of different sizes and urbanization levels are selected as study areas. The urban centers

Manuscript received March 19, 2020; revised May 15, 2020 and June 11, 2020; accepted June 13, 2020. Date of publication June 18, 2020; date of current version July 2, 2020. This work was supported by the Foundation of the Key Program of the National Natural Science Foundation of China under Grant 41331171. *(Corresponding author: Xihan Mu.)*

The authors are with the Faculty of Geographical Science, Beijing Engineering Research Center for Global Land Remote Sensing Products, Institute of Remote Sensing Science and Engineering, Beijing Normal University, Beijing 100875, China, and also with the State Key Laboratory of Remote Sensing Science, Jointly Sponsored by Beijing Normal University and Institute of Remote Sensing and Digital Earth of Chinese Academy of Sciences, Beijing 100875, China (e-mail: xuejunw@mail.bnu.edu.cn; muxihan@bnu.edu.cn; gjyan@bnu.edu.cn).

Digital Object Identifier 10.1109/JSTARS.2020.3003480

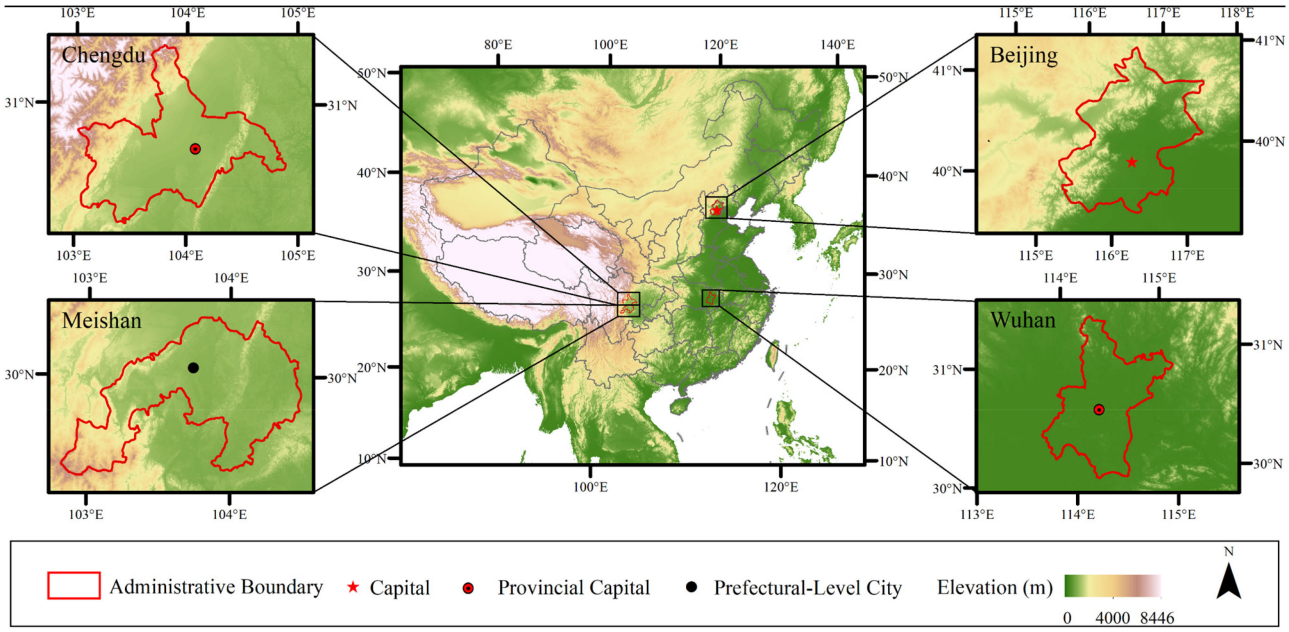

Fig. 1. Study areas.

TABLE I
INFORMATION OF STUDY AREAS

City	Land Area (km^2)	Average PM2.5 in 2015 ($\mu g/m^3$)	Urban Population (10000 persons)	Urbanization Rate [a] (%)	Climate
Beijing	16410.54	81	1876.6	86.45	Temperate semi-humid continental monsoon
Wuhan	8569.15	70	871.87	80.04	Subtropical humid southeast monsoon
Chengdu	14335	64	1152.81	71.85	Subtropical humid southeast and southwest monsoon
Meishan	7134	62	133.18	44.77	Similar to that of Chengdu

[a]The proportion of the urban population to the total population. Data are obtained from the statistical yearbook for 2017 of four cities.

are extracted and then two regression formulas are applied to evaluate the relationship between the NTL radiance and AOD. The VIIRS DNB NTL data are adopted to study the quantitative impact of aerosols.

The rest of this article is organized as follows. Section II introduces the study areas and data used. The data preprocess procedure, extraction of urban centers, statistical analysis, and linear regression are described in Section III. Results and discussion are found in Sections IV and V, respectively, and the conclusion is presented in Section VI.

II. Study Areas and Data

A. Study Areas

The four cities under the study include Beijing in northern China, representing a highly urbanized and developed city. Chengdu in western China and Wuhan in central China are the respective capitals of Sichuan and Hubei provinces, representing large cities and regional economic centers. Meishan is a middle-sized city in Sichuan Province, representing the cities undergoing the urbanization (see Fig. 1 and Table I).

Beijing (39.4°–41.6°N, 115.7°–117.4°E) is the capital of China and is located in the northern part of the North China Plain. This area is characterized by a monsoon-influenced semihumid continental climate and features a high-temperature rainy summer, cold and dry winter, and short spring and autumn. Beijing is one of the largest cities in the world and has become heavily polluted due to the rapid urbanization and industrialization over the past two decades [38]. Systematic measures, such as the desulfurization treatment in coal-fired power plants [42] and upgrading fuels for vehicles [43], have been applied. Thus, air pollution has been alleviated in recent years.

Wuhan (29°58′–31°22′N, 113°41′–115°05′E) is located in the eastern part of the Jianghan Plain and at the intersection of the Yangtze and Han rivers. This area is a subtropical humid southeast monsoon climate zone with abundant rainfall and heat, cold winter and hot summer, and distinct four seasons. Chengdu (30°5′–31°26′N, 102°54′–104°53′E) is located in the western part of Sichuan Basin and the eastern edge of Qinghai–Tibet Plateau. The overall terrain is high in the northwest and low in the southeast. Chengdu is a subtropical humid and semihumid monsoon climate zone with a mild climate, long frost-free period, abundant rainfall, and limited sunshine. Meishan (29°24′–30°16′N, 102°49′–104°30′E) is located in the southwestern part of the Chengdu Plain in the Sichuan Basin and the climate is similar to that of Chengdu. The city is a vast plain with the

mountainous area in the west and hilly area in the east. The details are illustrated in Table I.

B. VIIRS Data

The Earth Observation Group in the National Oceanic and Atmospheric Administration's National Geophysical Data Center (NOAA/NGDC) of the United States released the monthly global NTL composite data from the VIIRS DNB. Data from August 2015 to December 2018 were downloaded[1] to analyze the relationship between the NTL radiance and AOD. Each monthly tarball contained two files, namely, the average DNB radiance and the average number of cloud-free (NCF) observations. The "vcmcfg" version of the data was used at a resolution of 15 arcsecond (approximately 500 m) grids and radiance values with the units in $nW \cdot cm^{-2} \cdot sr^{-1}$. These data were produced by the averaging values of the DNB band after excluding data near the edges of the swath and data impacted by twilight, stray light, lightning, lunar illumination, and cloud cover [44].

To estimate the aerosol effect on daily NTL radiance, the year 2016 was studied and data from the NOAA comprehensive large array-data stewardship system were downloaded. Four types of VIIRS data were used in this study, which are as follows:

1) VIIRS/DNB sensor data record data (SVDNB);
2) VIIRS/DNB geographical sensor data record data (GDNBO);
3) VIIRS cloud-aggregated environment data record ellipsoid geolocation environment data record data (GCLDO);
4) VIIRS cloud cover layers environment data record data (VCCLO).

The SVDNB data provided the NTL radiation information. The GDNBO data provided the corresponding geographic information for the SVDNB radiance image. The GCLDO and VCCLO data were used to judge whether the clouds would appear at night, so as to screen out the cloudless night. Each SVDNB radiance image had a swath of approximately 3060 km, which had been processed with a radiometric calibration and stray light correction from the raw DNB radiance data [45].

C. AERONET Aerosol Data

The AERONET observation instrument provides the long-term AOD information in different regions of the world with an uncertainty lower than 0.02 [46]. Every 15 min, the AERONET measures the AOD of central wavelengths, which are 340, 380, 440, 500, 675, 870, 940, and 1020 nm. The AOD data are available at three data quality levels (levels 1.0, 1.5, and 2.0) and three temporal scales (15 min, daily, and monthly). Level 2.0 AOD data are processed with the prefield and postfield calibration, cloud screening, and quality control. In this study, Version 3 Level 2.0 AOD data with the enhanced cloud screening and quality assurance [47] at the Beijing (39.98 N, 116.38 E) and Beijing CAMS (39.93 N, 116.32 E) sites are used to evaluate the aerosol effect on NTL, including the daily data of 2016 and monthly data from August 2015 to December 2018. This study used the mean AOD of the two sites at 500 nm, which was consistent with the Himawari products introduced in the following section.

D. Himawari Aerosol Products

Himawari-8 is a new-generation meteorological satellite launched by the Japan Meteorological Agency, Tokyo, Japan, on October 7, 2014. The advanced Himawari imager has a wide range of wavelengths, including 16 bands from the visible to infrared wavelengths and 10 min observation frequency of the full disk [48]. This satellite also provides 10 min, hourly, daily, and monthly variability of AOD over Asia and Oceania. In this study, Level 3, Version 3 daily, and monthly AOD are downloaded from.[2] The resolution of the AOD is 0.05° at a wavelength of 500 nm and the subdataset named AOT_L2_Mean is used. The detailed information about the products can be found in the document.[3]

Beijing, as a highly urbanized capital city, generally attracts high public attention and its AOD-related data are the most abundant among the four cities. The quantitative analyses of NTL radiance and AOD in Beijing are conducted with daily and monthly data. By contrast, the other three cities have no AERONET sites as yet and, thus, are analyzed using the monthly Himawari AOD. Since only the daytime AOD can be obtained from AERONET and Himawari, the AOD of two successive days (before and after the VIIRS nighttime overpass) were averaged for the analysis.

III. Methods

A. Data Preprocessing

All the spatial data (including remotely sensed and administrative boundary data) were resampled to the same spatial resolution as VIIRS DNB monthly composites (0.0041667°). The daily NTL radiance data that did not contain all of Beijing were excluded. Unlike the well-processed monthly NTL data produced by NOAA/NGDC, the daily NTL data were checked using the following flowchart, as shown in Fig. 2.

1) Step 1: The solar zenith angle (SZA) information from the GDNBO product was extracted and the NTL radiance data with SZA $< 101°$ were discarded to remove the impact of the sunlight [33]. To exclude the NTL images contaminated by the moonlight, the local moonrise and moonset time information[4] were used, and then the data without the moonlight contamination were selected.
2) Step 2: Cloud cover data were extracted using the VCCLO. According to these data, the clouds were masked and then the NTL radiance data without sunlight, clouds, and bad data were selected.
3) Step 3: The VIIRS can revisit a place more than once every night because of the design of the satellite orbit. Two NTL images acquired in the same area within one night were combined by average to acquire the daily processed data. Similarly, the satellite viewing zenith angle

[1]Online. [Available]: https://eogdata.mines.edu/download_dnb_composites.html

[2]Online. [Available]: https://www.eorc.jaxa.jp/ptree/terms.html

[3]Online. [Available]: https://www.eorc.jaxa.jp/ptree/documents/Himawari_Monitor_Aerosol_Product_v5.pdf

[4]Online. [Available]: https://sunrisesunsetmap.com

TABLE II
REGIONAL SCREENING CRITERIA AND RESULTS OF DIFFERENT CITIES

City	Beijing	Wuhan	Chengdu	Meishan
Light Threshold ($nW \cdot cm^{-2}sr^{-1}$)	14.145	16.88	21.7	10.41
Mean Value of Urban Area ($nW \cdot cm^{-2}sr^{-1}$)	27.035	26.329	36.793	16.722
Pixel Counts	7044	2271	2134	104
Proportion of Impervious Surface (%)	66.41	75.55	75.50	69.70

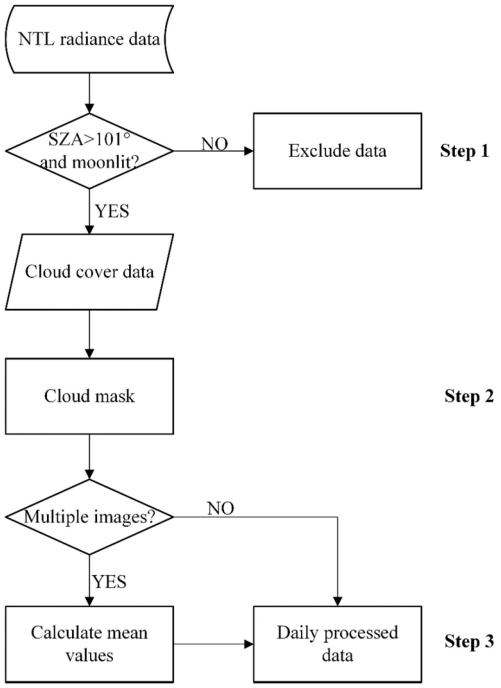

Fig. 2. Flowchart for checking the daily NTL radiance data.

(VZA) extracted from GDNBO was also processed using Steps 1 and 2. In addition, Himawari daily AOD at the urban center of Beijing in 2016 were masked according to the corresponding NTL images to ensure the regional consistency in the subsequent analysis. The masked daily AOD with less than 1000 pixels were excluded.

B. Extraction of Urban Centers

With dense buildings, well-developed transportation, and more human activities, the urban centers are illuminated artificially at night, and their corresponding pixels in the NTL images have the larger radiance values than the surrounding suburban countryside. Moreover, urban expansion is generally centered on the old city, which has not changed significantly over time. The local overpass time of the NPP satellite at night is approximately 1:30 A.M. when most of the residential indoor lights have been turned OFF. The main light sources are the street and infrastructure lights, which may not change much with time [49], and thus, the light background value of this area can be assumed to remain the same.

Shi *et al*. [18] extracted the built-up urban areas with the light synthesis data of 2012 (April 18–26, 2012 and October 11–23, 2012) and obtained the light thresholds of different cities (see Table II). This study extracts the urban centers based on these thresholds. The details of the processes are described as follows.

1) Acquisition of urban pixels: Any pixel in the monthly light synthesis data of April 2012 with the radiance exceeding the threshold was identified as a city pixel. After the threshold screening, areas with fragments were obtained.
2) Region of interest extraction: Small fragments were deleted and the largest zone was retained. Several small void pixels (one or several pixels were not selected) were placed in the zone and the vector boundaries were obtained for the urban centers of four cities, as shown in Fig. 3.
3) NTL data of urban centers: Using the vector files to extract all the NTL images, a series of the urban center NTL data were obtained. Similarly, NCF, Himawari daily AOD, Himawari monthly AOD data, and 10-m-resolution land cover data [50] were masked using vector files. Table II illustrates the NTL data acquired at the four urban centers (April 2012) and the proportions of the impervious surface (2017). Fig. 3 shows the extraction results of the urban centers of four cities, among which the urban center of Beijing is the largest and that of Meishan is the smallest. The proportions of the impervious surface of the four cities are all approximately 70%.
4) The regional average radiance $I$and logarithm of the radiance $\ln(I)$for all the NTL radiance data of the urban centers were calculated. Furthermore, the regional average values of NCF data were calculated and the monthly NTL data with values lower than 3 were discarded.

C. Statistical Analysis of NTL Radiance Distribution

Anomaly is the deviation of a value from the mean of a dataset. Based on the mean value of the daily AOD of Beijing in 2016, the AOD anomaly (AOD_d) was calculated. According to the AOD_d range, the aerosol pollution was divided into five levels (Level 1– 5), i.e., relatively clean, lightly polluted, moderately polluted, heavily polluted, and severely polluted. Then, the box plot, also known as the box-whisker plot, was applied to measure the NTL radiance distribution according to the graded AOD. The box plot describes data using its five statistics: minimum, first quartile, median, third quartile, and maximum.

D. Modeling the Aerosols Effect

The relationship between the NTL radiance and AOD is analyzed using two models, namely, linear regression (LR) and log-linear regression (L-LR). The ordinary least squares algorithm is widely used to fit the regression models. The LR

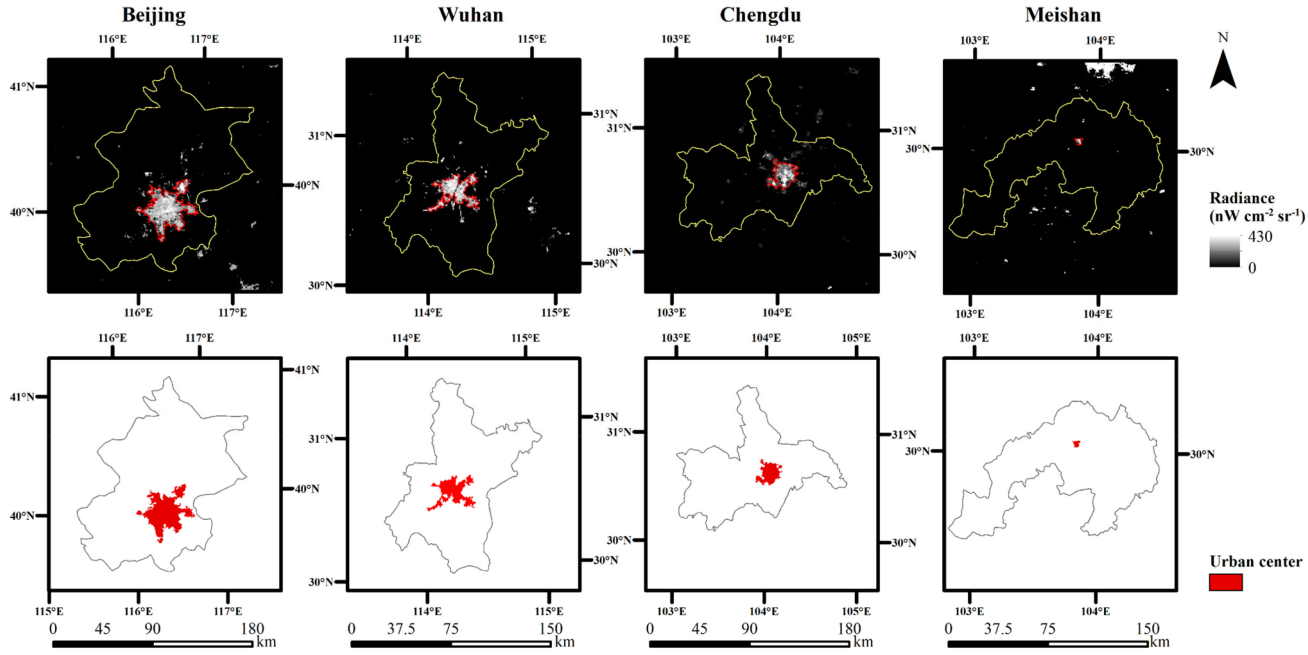

Fig. 3. Urban centers of the four cities.

model is as follows:

$$I = a\tau + b \tag{1}$$

where I is the radiance that the DNB sensor received, τ is the total optical depth, and a and b are the coefficients. τ consists of Rayleigh scattering optical depth τ_{ray}, unscreened cirrus optical depth τ_c, and aerosol optical depth τ_{aer}. We assume that τ_{ray} is relatively stable and VIIRS DNB data are cloud free after the cloud mask. Thus, τ is equivalent to τ_{aer}.

If the effects of the cloud and moonlight are removed, the radiance received by the satellite sensor only includes part of the ground light source. Ignoring the contributions from the multiple scattering effects and considering the differences of viewing geometries between various nights, the relationship between τ and I can be expressed in the following formula [19], [23]:

$$I = I_0 e^{-\tau/\mu} \tag{2}$$

where I_0 is the initial (unattenuated) upwelling radiance from the surface light source (artificial light) and μ is the cosine of the VZA. Then, a simplified radiation transfer equation (L-LR) is made.

$$\ln(I) = a\tau + b. \tag{3}$$

Equation (1) is approximately equivalent to (3) when a is small.

The effect of VZA on the NTL data is also analyzed using a more complicated model. Li *et al.* [51] discovered the relationship between the artificial light radiance and satellite viewing angles by using the daily NTL images and used a quadratic model as in (4) to remove this impact. Combining (2) and (4), a model is reconstructed to jointly consider VZA and AOD

$$I_0 = a\theta^2 + b\theta + c \tag{4}$$

$$I = \left(a\theta^2 + b\theta + c\right) e^{d\tau/\cos(\theta)} \tag{5}$$

where θ denotes the VZA and a, b, c, and d are the coefficients.

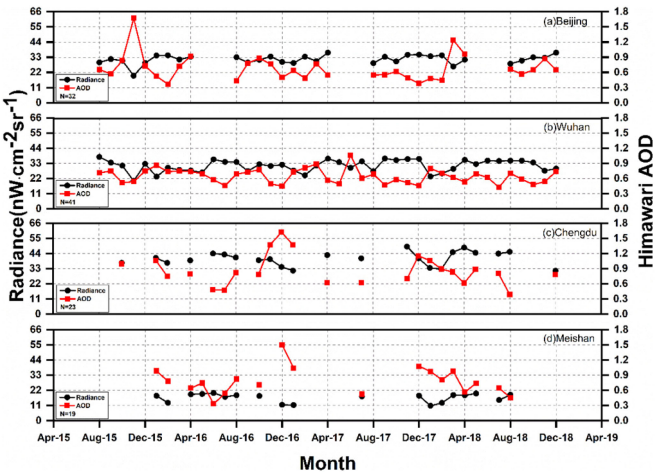

Fig. 4. Monthly series of the NTL radiance and AOD for the four cities. (a) Beijing. (b) Wuhan. (c) Chengdu. (d) Meishan.

IV. Results

A. Time Series of NTL Radiance and AOD

Fig. 4 shows the monthly series change of the NTL radiance and AOD of four cities. Beijing's monthly NTL composites of May, June, and July are missing due to poor data quality. The monthly series image shows that the NTL radiance and

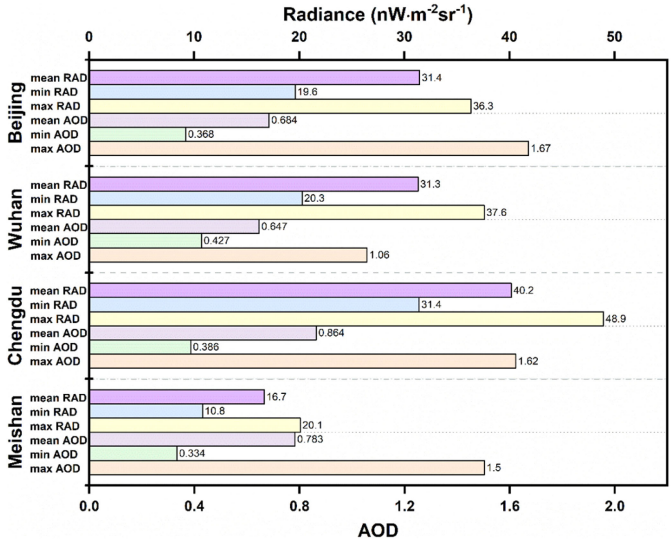

Fig. 5. Statistics of the monthly NTL radiance and Himawari AOD information of the four cities. RAD represents the NTL radiance.

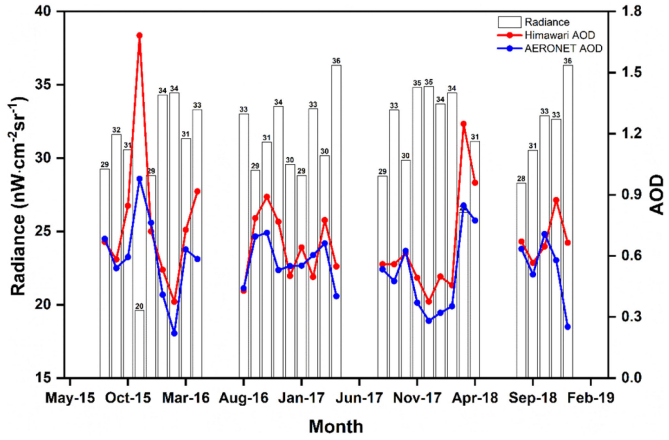

Fig. 6. Monthly change of the NTL radiance and AOD in Beijing. The red and blue lines represent the monthly Himawari AOD and AERONET AOD, respectively. The NTL radiance is shown with the histogram.

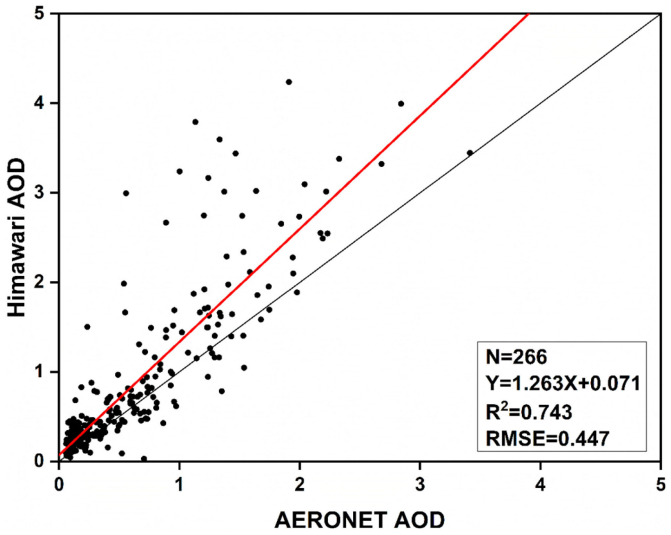

Fig. 7. Comparison of the daily Himawari and AERONET AOD (Beijing CAMS site) in 2016. The red and black lines represent the linear trend line and the 1:1 line, respectively.

AOD generally show an opposite change trend. The minimum radiance values for Beijing and Wuhan are in November 2015, while those of Chengdu and Meishan are in December 2018 and January 2018, respectively.

As is shown in Fig. 5, the relationship among the monthly mean NTL radiance of four urban centers is Chengdu > Wuhan > Beijing > Meishan and that among the Himawari AOD is Chengdu > Meishan > Beijing > Wuhan. The ranges of the NTL radiance are 19.6–36.3 nW.m^{-2}sr^{-1}, 20.3–37.6 nW.m^{-2}sr^{-1}, 31.4–48.9 nW.m^{-2}sr^{-1}, and 10.8–20.1 nW.m^{-2}sr^{-1} for Beijing, Wuhan, Chengdu, and Meishan, respectively. All variation ranges of the NTL radiance are higher than 15 nW.m^{-2}sr^{-1} except for that of Meishan. The ranges of monthly AOD are 0.368–1.67, 0.427–1.06, 0.386–1.62, and 0.334–1.50 for Beijing, Wuhan, Chengdu, and Meishan, respectively. The variation ranges of AOD are larger than one except for that of Wuhan.

Fig. 6 shows the monthly series change of the NTL radiance and AOD in Beijing. Both AERONET and Himawari AOD exhibit negative correlations with the NTL radiance. The lowest radiance value is in December 2015 and the corresponding AOD is the largest. From the second half of 2015 to the first half of 2016, the NTL radiance of Beijing shows considerable fluctuations. The NTL radiance distinctly increases, especially from November 2015 to February 2016. Fig. 6 shows that the change trends of the two types of AOD are similar, although Himawari AOD is generally higher than AERONET AOD. Further analysis shows that a similar result of the daily comparison of AERONET and Himawari AOD in Beijing and R^2 is 0.743, and the root-mean-squared error (RMSE) is 0.447 (see Fig. 7). R^2 and RMSE are both higher than those in [52].

B. Analysis of NTL Radiance and AOD of Beijing

Based on the average value of the daily AOD of Beijing in 2016, the AOD$_d$, i.e., the deviation from the average, is adopted to represent the change of AOD and air cleanliness. The ranges of AOD$_d$ are within −0.7–0.7 except for a few larger values. Therefore, the AOD$_d$ is divided into five levels according to the criteria given in Table III.

TABLE III
GRADED AOD ANOMALY FOR BEIJING

AOD$_d$ range	Air pollution level	Defined pollution level
AOD$_d \le -0.4$	Relatively clean	Level-1
$-0.4 <$ AOD$_d < -0.1$	Lightly polluted	Level-2
$-0.1 \le$ AOD$_d < 0.1$	Moderately polluted	Level-3
$0.1 \le$ AOD$_d < 0.4$	Heavily polluted	Level-4
AOD$_d \ge 0.4$	Severely polluted	Level-5

To illustrate the effect of AOD on the NTL radiance, the box plot is applied to show the variation of the NTL radiance distribution among different AOD levels. The results are derived using AERONET and Himawari AOD, as shown in Fig. 8. The "box," including its inner line, solid circle, and whisker, has a significant change at different AOD$_d$ levels. As the AOD

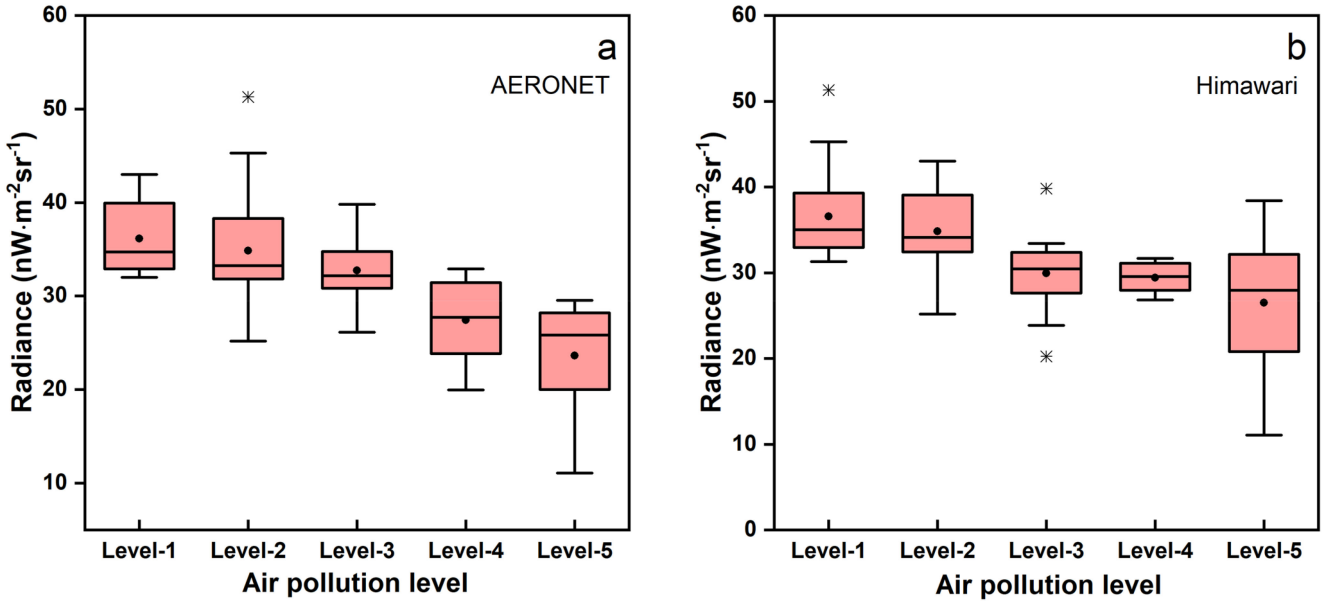

Fig. 8. Box plots of the daily NTL radiance against the graded air pollution level. (a) AERONET. (b) Himawari. For each level, the following descriptive statistics are shown: minimum, 25th quartile, median, mean, and 75th quartile with the limits (ends of the "whiskers") beyond which the values are considered anomalous (displayed as black stars). The mean is displayed with a black dot and a black line (in the middle of the box) corresponds to the median.

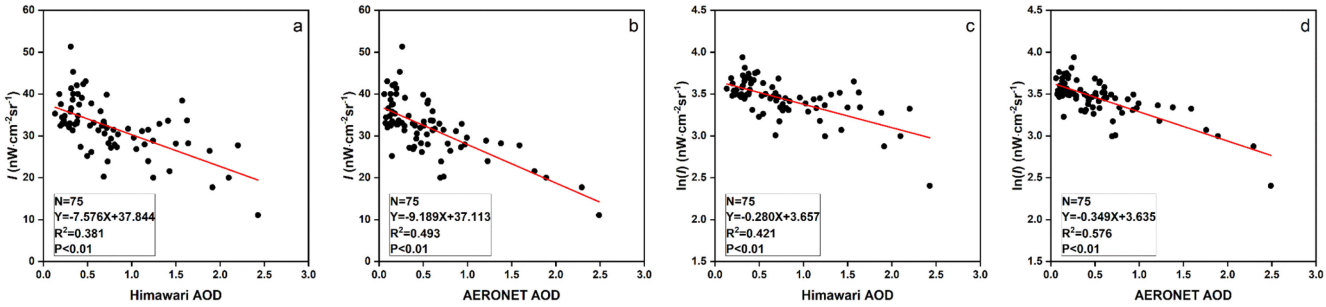

Fig. 9. Relationship of the daily NTL radiance and AOD in Beijing. (a) and (b) using the LR regression model, and (c) and (d) using the L-LR regression model. The red lines denote the trend lines.

increases (from Level 1 to Level 5), the mean and median decrease, which suggests an opposite trend between the NTL radiance and aerosols. The 75th percentile of Fig. 8(a) and the 25th percentile of Fig. 8(b) also show a similar trend to the mean. The box sizes for Fig. 8(a) and (b) vary because of the difference between the two AOD products.

The relationship of the daily NTL radiance and AOD is shown in scatter plots (see Fig. 9). The radiance decreases with the increase of AOD for both AERONET and Himawari. The R^2 values of 0.381 and 0.493 are obtained using the LR model for AERONET and Himawari, respectively ($P < 0.01$). The R^2 of 0.421 and 0.576 are obtained using the L-LR model for AERONET and Himawari, respectively ($P < 0.01$).

The monthly analysis was carried out for the aerosol effects on NTL data. Fig. 10 shows the relationship between the NTL radiance and AOD by fitting with the LR and L-LR models.

The NTL radiance decreases as AOD increases. The R^2 values of 0.527 and 0.655 are obtained using the LR model for Himawari AOD and AERONET AOD, respectively. R^2 changes less than 0.05 by using the L-LR model. The results are statistically significant ($P < 0.01$) and show that the relationship between the NTL radiance and AOD is quasilinear.

Table IV lists the Pearson correlation coefficient r and the corresponding coefficients a and b. The r values are lower than -0.61 and verified the negative correlation between the NTL radiance and AOD. The results using the L-LR model are almost slightly larger than those obtained using the LR model, suggesting that the simplified radiation transfer equation can slightly better represent the relationship between the NTL radiance and AOD. For the LR model, the slope a of the linear function for Himawari AOD is less than that for AERONET AOD, indicating their difference (see Fig. 7, Himawari AOD overall is larger than AERONET AOD). The monthly a values are larger than the daily a values. In general, the b values are almost consistent for each model.

C. Comparative Analysis of Different Cities

The LR and L-LR models are used to fit the NTL radiance and AOD of the four urban centers. As shown in Fig. 11, the order

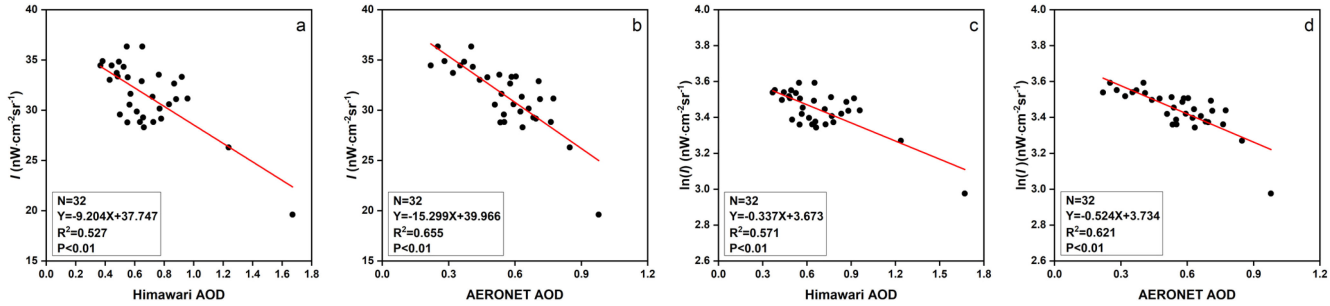

Fig. 10. Relationship of the monthly NTL radiance and AOD in Beijing. (a) and (b) using the LR regression model, and (c) and (d) using the L-LR regression model. The red lines denote the linear trend lines.

TABLE IV
RELATIONSHIP BETWEEN THE NTL RADIANCE AND AOD OF BEIJING

Model	AOD Product	Time Scale	r	R^2	a	b
LR	AERONET	Daily	−0.702*	0.493	−9.189	37.113
	Himawari	Daily	−0.617*	0.381	−7.576	37.844
	AERONET	Monthly	−0.809*	0.655	−15.299	39.966
	Himawari	Monthly	−0.726*	0.527	−9.204	37.747
L-LR	AERONET	Daily	−0.759*	0.576	−0.349	3.635
	Himawari	Daily	−0.649*	0.421	−0.280	3.657
	AERONET	Monthly	−0.788*	0.621	−0.524	3.734
	Himawari	Monthly	−0.756*	0.571	−0.337	3.673

∗denotes that the correlation is significant at 0.01 level.

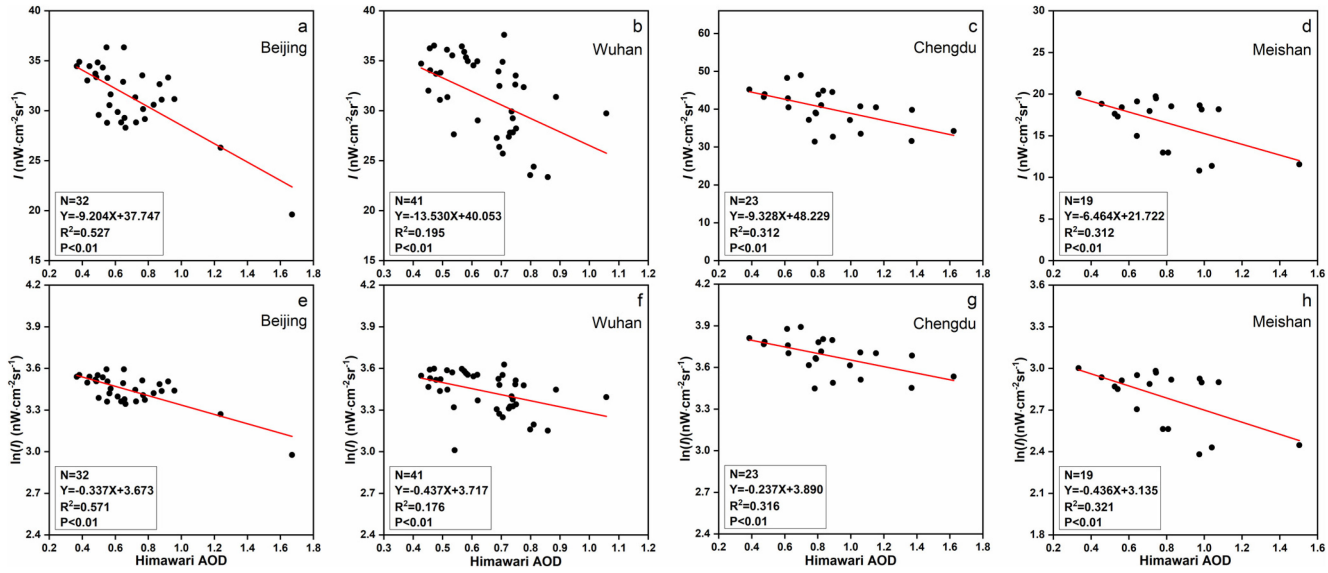

Fig. 11. Scatter plots of the radiance and Himawari AOD using the (a)–(d) LR model and the (e)–(h) L-LR model for the four cities.

of a values is Wuhan (13.530) > Chengdu (9.328) > Beijing (9.204) > Meishan (6.464) for the LR model and Wuhan (0.437) > Meishan (0.436) > Beijing (0.337) > Chengdu (0.237) for the L-LR model. The order of b values in the LR and L-LR models is Chengdu (48.229, 3.890) > Wuhan (40.053, 3.717) > Beijing (37.747, 3.673) > Meishan (21.722, 3.135), which is similar to the order of the threshold used to determine the urban centers (see Table II). Fig. 12 shows similar R^2 values for the two models, whereas the R^2 value in each urban center varies significantly. For example, the R^2 obtained using the L-LR model for Beijing is 0.571, while that for Wuhan is 0.176.

D. Influence of Anisotropic Effect

The daily NTL radiance is obtained at a specific viewing angle, which changes every day. Equation (5) is used to describe the joint effects of VZA and AOD on the NTL radiance with the daily data acquired in Beijing, as shown in Fig. 13. As the

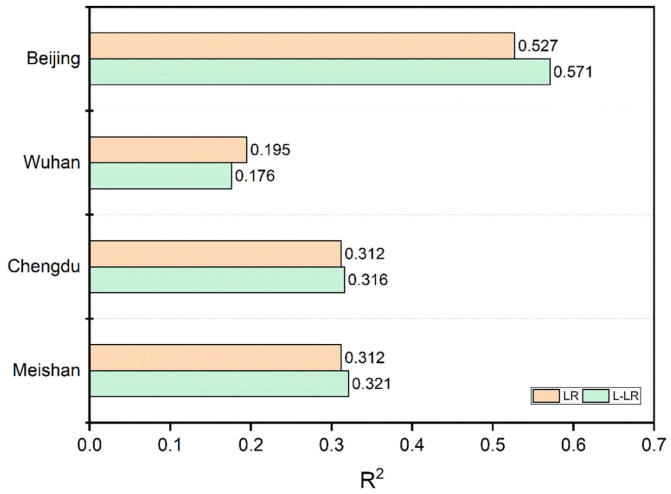

Fig. 12. R^2 values of the LR and L-LR models for the four cities.

AOD increases, the NTL radiance decreases. In addition, the NTL radiance is relatively high when VZA is large. The R^2 values are 0.497 and 0.635 for Himawari AOD and AERONET AOD, respectively, and are slightly larger than those using the L-LR model (0.421 and 0.576 in Table IV), suggesting that the consideration of VZA slightly improves the correlation between the daily NTL radiance and AOD. The coefficient d of the two equations in (5) and Fig. 13 is almost the same as b values in the LR model (about 37 in Table IV) and can also express the unattenuated upwelling radiance from the surface light source I_0.

V. Discussion

A. Potential Impact of AOD on the Application of NTL Data

The VIIRS DNB data can be used in feature detection, fire monitoring, urban expansion research, and population estimation, which all need the thresholds to recognize and discriminate NTL of different areas. These thresholds are easily affected by aerosols in the atmosphere and may show a blooming effect strengthened by the scattering of the aerosol particles in VIIRS DNB data [53]. In this study, the quantitative analyses are carried out on the relationships of the NTL radiance and AOD in Beijing and three other cities of different development stages. The relationship between the NTL radiance and AOD suggests that the radiance may decrease by over 15 nW.cm^{-2}sr^{-1} when AERONET AOD increases one unit (for Beijing in Table IV). This amount is higher than the threshold of urban areas (14.145 nW.cm^{-2}sr^{-1}) obtained using the published methods [18], indicating the considerable atmospheric effect on NTL data. Equations (1) and (3) indicate that the coefficient b in the LR model and e^b in the L-LR model are in essence the initial upwelling radiance from the surface light source I_0 and a represents the sensitivity of the NTL radiance to AOD. The upwelling radiance from the surface light source highly varies among the cities (the NTL radiance of Meishan is half as those of others in Fig. 4). By contrast, the slope a is the second-largest for Meishan among the four cities using the L-LR model (see Fig. 11), showing that the sensitivity of the NTL radiance to AOD is relatively independent of the initial upwelling NTL radiance. Therefore, the regression coefficients constructed with AOD are potentially valuable in the correction of the atmospheric effects in NTL data.

B. Other Related Factors

The relationship between the NTL radiance and AOD is also affected by several factors, including the temporal and spatial characteristics of data, types of AOD, and regression models.

1) Time Scale of Data: The R^2 of the monthly results are higher than those of the daily results in Table IV. Although the VIIRS DNB data released by NOAA have undergone geometric correction, radiometric calibration, and stray light removal [45], numerous factors influence the uncertainty of the daily NTL data compared with the monthly NTL data. Li *et al.* [51] analyzed the relationship between the radiance and satellite viewing angles using the daily NTL images. Both I and I_0 are the functions of VZA. Given the periodicity of the satellite orbit, the monthly NTL data tend to mitigate the angle effect. Another reason is the existence of statistical deviations. The data of the low polluted atmosphere have a high data quality and are prone to be selected, causing the daily datasets to mainly concentrate on the low AOD values (see Fig. 9). The monthly aggregation increases the uniform distribution of the AOD data, which may enhance the correlation between the NTL radiance and AOD.

2) Difference of Cities: The NTL radiance values of Beijing, Wuhan, and Chengdu are similar but that of Meishan is much lower. Given the rainy weather in Chengdu and Meishan, less NTL composite data are available than those for Beijing and Wuhan. The R^2 value of Wuhan is less than the other three cities and the largest is for Beijing (see Fig. 12). The AOD level for Wuhan is the lowest among the four cities (see Fig. 5), resulting in a weak correlation between the NTL radiance and AOD. Beijing is located in a basin, promoting the accumulation of air pollutants and limiting their dispersion. Similarly, Chengdu and Meishan are located in the Sichuan Basin, which is also not conducive to the diffusion of pollutants. Thus, the NTL radiance change caused by AOD is more prominent and the correlation is higher. In fact, the DNB band (500–900 nm) contains the effect of the water vapor absorption that thereby affects the a values. Compared with the other three cities, Beijing is relatively dry and the influence of the water vapor is smaller. The a values of the three large cities are higher than those of Meishan, as shown in Fig. 11(a)–(d), suggesting that AOD may have a greater impact on the NTL radiance of the cities with high urbanization levels. The results imply that the relationship between the NTL radiance and AOD varies among the cities of different urbanization levels and climate types.

3) Different AOD Products: We can see from Table IV that the slope value a derived from the NTL radiance and Himawari AOD is generally smaller than that derived from the NTL radiance and AERONET AOD. This is caused by the overestimation of Himawari AOD, as shown in Figs. 6 and 7, also in agreement with Zhang *et al.* [52]. The AOD of AERONET is more reliable than Himawari AOD, therefore, the regression

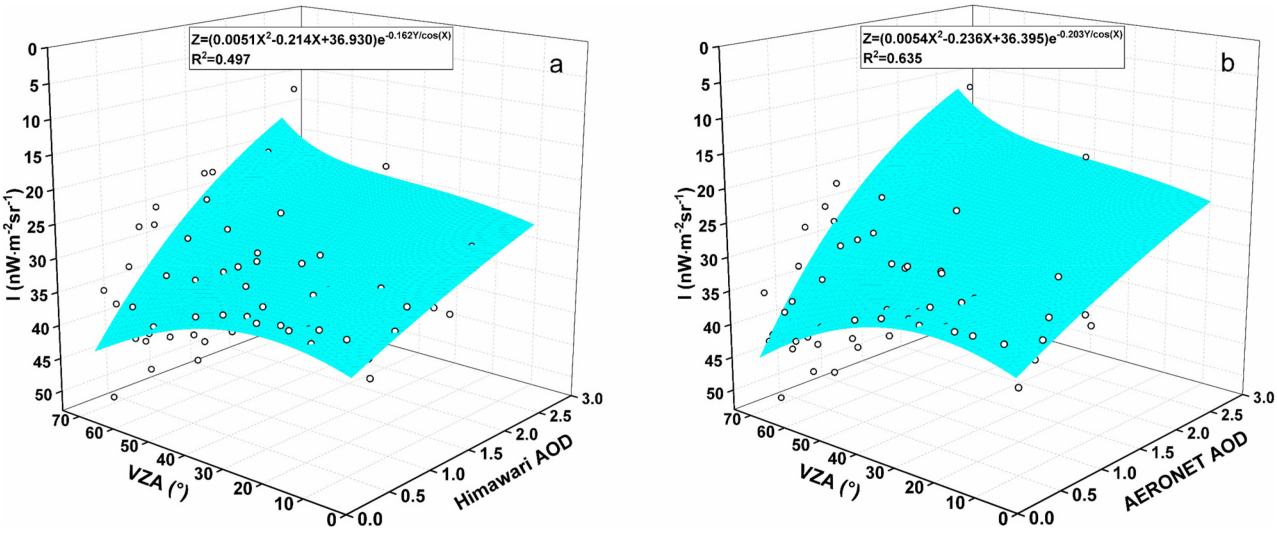

Fig. 13. Fitting of NTL radiance, VZA, and AOD. (a) Himawari AOD. (b) AERONET AOD. The blue surfaces are fitted using (5). *X*, *Y*, and *Z* represent VZA, AOD, and NTL radiance, respectively.

relationship obtained by AERONET is relatively more accurate. Future updates on the aerosol retrieval methods with satellite data can help promote the fitting accuracy of NTL data and AOD.

4) Difference of Regression Models: Fig. 12 and Table IV illustrate that the R^2 values obtained using the L-LR model are slightly larger than those obtained using the LR model (the improvement is less than 0.05), suggesting that the simplified radiation transfer equation (2) can slightly better represent the relationship between the NTL radiance and AOD. In essence, this relationship is logarithmic and is also used to retrieve AOD [19], [20], [23], [54]. However, a description with the linear fitting is simpler and can largely reflect the relationship.

C. Limitations

In this study, the LR model is used to analyze the relationship between the NTL radiance and AOD. The Pearson correlation coefficient of Beijing is approximately 0.8, yet this value is not very high overall and even smaller for other cities, suggesting that aerosols cannot account for all the radiance changes in urban centers. The possible reasons are as follows.

1) The daytime AOD used in this study may have a certain difference with the nighttime AOD [55].
2) The NTL background values of the urban centers are assumed to be unchanged with time because the NTL data were obtained at midnight when the human activities are reduced. Uncertainties also exist, such as socio-economic development or extreme short-term events [28].
3) The changes in the land cover can result in the seasonal changes of the NTL radiance in the long term [56]. Although the urban centers extracted are mostly covered by the impervious surface (see Table II), vegetation changes influence the NTL radiance, especially in Beijing that has deciduous forests with four distinct seasons.
4) The VIIRS DNB data contain information in a wide range of the wavelength from 500–900 nm, where the oxygen *A*-band and other absorbing bands, such as water vapor [19].
5) The uncertainty caused by an unscreened cirrus cloud is ignored. Passive radiometric satellite products are contaminated by the cirrus cloud about 25% of the time [57]. The unscreened cirrus cloud may cause a radiance attenuation in the NTL data.

D. Suggestions for Future Work

In view of the factors mentioned above, several improvements can be used in future research. First, the nighttime atmospheric data observed from CALIPSO [58] and the new sun-sky-lunar Cimel CE318-T multiband photometer [59] can be used to analyze the relationship between the nighttime aerosols and NTL radiance. Second, the impact of short-term events and long-term seasonal changes of both AOD and NTL data need consideration. Third, although the AERONET AOD represents the ground truth and the accuracy is high, the spatial representation of sites remains to be discussed. Finally, more cities are needed to reveal the aerosol effect on the NTL radiance and the feasibility of using the AOD data to remove the atmospheric effect on NTL data.

VI. Conclusion

The change of the NTL radiance contains the signals of air pollution, which influence the quantitative application of NTL data. The atmospheric effect requires consideration and the corresponding correction is necessary before the application of NTL data. Two regression models are applied to detect the relationship between the NPP-VIIRS NTL radiance and AOD of AERONET and Himawari. The results suggest that changes in the NTL radiance are negatively correlated with the changes of AOD for the urban centers of four different cities in China. The correlation is strongest in Beijing, where a high Pearson correlation coefficient (approximately -0.8) was obtained in the monthly analysis. The NTL radiance may decrease by 10 $\mathrm{nW.cm^{-2}sr^{-1}}$ as the daily AERONET AOD increases by one unit. This decrease

may reach above 15 nW.cm^{-2}sr^{-1} for the monthly AERONET AOD. The comparison shows the influence of AOD in cities with different sizes, climate types, and development stages. This influence is prominent for cities with a high urbanization level and dry climate.

ACKNOWLEDGMENT

The authors would like to thank the monthly global NTL composite data from the VIIRS DNB provided by the Earth Observation Group of Payne Institute, VIIRS data provided by the NOAA Comprehensive Large Array-Data Stewardship System, H8/AHI data provided by the Japan Aerospace Exploration Agency, and AERONET data maintained by the Institute of Atmospheric Physics, Chinese Academy of Sciences (Beijing site), and Chinese Academy of Meteorological Science (CMAS site).

REFERENCES

[1] M. M. Bennett and L. C. Smith, "Advances in using multitemporal nighttime lights satellite imagery to detect, estimate, and monitor socioeconomic dynamics," *Remote Sens. Environ.*, vol. 192, pp. 176–197, 2017.

[2] C. D. Elvidge, K. E. Baugh, M. Zhizhin, and F. C. Hsu, "Why VIIRS data are superior to DMSP for mapping nighttime lights," in *Proc. Asia-Pacific Adv. Netw.*, 2013, vol. 35, pp. 62–69.

[3] L. Coscieme, F. M. Pulselli, S. Bastianoni, C. D. Elvidge, S. Anderson, and P. C. Sutton, "A thermodynamic geography: Night-time satellite imagery as a proxy measure of emergy," *Ambio*, vol. 43, pp. 969–979, Nov. 2014.

[4] T. Ma, C. Zhou, T. Pei, S. Haynie, and J. Fan, "Responses of Suomi-NPP VIIRS-derived nighttime lights to socioeconomic activity in China's cities," *Remote Sens. Lett.*, vol. 5, pp. 165–174, 2014.

[5] X. Chen and W. Nordhaus, "A test of the new VIIRS lights data set: Population and economic output in Africa," *Remote Sens.*, vol. 7, pp. 4937–4947, 2015.

[6] Z. Chen, B. Yu, Y. Hu, C. Huang, K. Shi, and J. Wu, "Estimating house vacancy rate in metropolitan areas using NPP-VIIRS nighttime light composite data," *IEEE J. Sel. Topics Appl. Earth Observ. Remote Sens.*, vol. 8, no. 5, pp. 2188–2197, May 2015.

[7] K. Shi *et al.*, "Modeling and mapping total freight traffic in China using NPP-VIIRS nighttime light composite data," *GISci. Remote Sens.*, vol. 52, pp. 274–289, 2015.

[8] B. Yu, K. Shi, Y. Hu, C. Huang, Z. Chen, and J. Wu, "Poverty evaluation using NPP-VIIRS nighttime light composite data at the county level in China," *IEEE J. Sel. Topics Appl. Earth Observ. Remote Sens.*, vol. 8, no. 3, pp. 1217–1229, Mar. 2015.

[9] N. Levin and Q. Zhang, "A global analysis of factors controlling VIIRS nighttime light levels from densely populated areas," *Remote Sens. Environ.*, vol. 190, pp. 366–382, 2017.

[10] C. D. Elvidge, M. Zhizhin, K. Baugh, and F.-C. Hsu, "Automatic boat identification system for VIIRS low light imaging data," *Remote Sens.*, vol. 7, pp. 3020–3036, 2015.

[11] C. Hu, S. Chen, M. Wang, B. Murch, and J. Taylor, "Detecting surface oil slicks using VIIRS nighttime imagery under moon glint: A case study in the Gulf of Mexico," *Remote Sens. Lett.*, vol. 6, pp. 295–301, 2015.

[12] W. C. Straka, C. J. Seaman, K. Baugh, K. Cole, E. Stevens, and S. Miller, "Utilization of the suomi national polar-orbiting partnership (NPP) visible infrared imaging radiometer suite (VIIRS) day/night band for Arctic ship tracking and fisheries management," *Remote Sens.*, vol. 7, pp. 971–989, 2015.

[13] T. N. Polivka, J. Wang, L. T. Ellison, E. J. Hyer, and C. M. Ichoku, "Improving nocturnal fire detection with the VIIRS day–night band," *IEEE Trans. Geosci. Remote Sens.*, vol. 54, no. 9, pp. 5503–5519, Sep. 2016.

[14] W. Guo, D. Lu, Y. Wu, and J. Zhang, "Mapping impervious surface distribution with integration of SNNP VIIRS-DNB and MODIS NDVI data," *Remote Sens.*, vol. 7, pp. 12459–12477, 2015.

[15] R. C. Sharma, R. Tateishi, K. Hara, S. Gharechelou, and K. Iizuka, "Global mapping of urban built-up areas of year 2014 by combining MODIS multispectral data with VIIRS nighttime light data," *Int. J. Digit. Earth*, vol. 9, pp. 1004–1020, 2016.

[16] Y. Dou, Z. Liu, C. He, and H. Yue, "Urban land extraction using VIIRS nighttime light data: An evaluation of three popular methods," *Remote Sens.*, vol. 9, 2017.

[17] B. Yu *et al.*, "Urban built-up area extraction from log-transformed NPP-VIIRS nighttime light composite data," *IEEE Geosci. Remote Sens. Lett.*, vol. 15, no. 8, pp. 1279–1283, Aug. 2018.

[18] K. Shi, C. Huang, B. Yu, B. Yin, Y. Huang, and J. Wu, "Evaluation of NPP-VIIRS night-time light composite data for extracting built-up urban areas," *Remote Sens. Lett.*, vol. 5, pp. 358–366, 2014.

[19] R. S. Johnson, J. Zhang, E. J. Hyer, S. D. Miller, and J. S. Reid, "Preliminary investigations toward nighttime aerosol optical depth retrievals from the VIIRS day/night band," *Atmos. Meas. Techn.*, vol. 6, pp. 1245–1255, 2013.

[20] T. M. McHardy, J. Zhang, J. S. Reid, S. D. Miller, E. J. Hyer, and R. E. Kuehn, "An improved method for retrieving nighttime aerosol optical thickness from the VIIRS day/night band," *Atmos. Meas. Techn.*, vol. 8, pp. 4773–4783, 2015.

[21] R. Li, X. Liu, and X. Li, "Estimation of the $PM_{2.5}$ pollution levels in beijing based on nighttime light data from the defense meteorological satellite program-operational linescan system," *Atmosphere*, vol. 6, pp. 607–622, 2015.

[22] Z. Xu, X. Xia, X. Liu, and Z. Qian, "Combining DMSP/OLS nighttime light with echo state network for prediction of daily $PM_{2.5}$ average concentrations in Shanghai, China," *Atmosphere*, vol. 6, pp. 1507–1520, 2015.

[23] J. Wang, C. Aegerter, X. Xu, and J. J. Szykman, "Potential application of VIIRS day/night band for monitoring nighttime surface $PM_{2.5}$ air quality from space," *Atmos. Environ.*, vol. 124, pp. 55–63, 2016.

[24] X. Zhao, H. Shi, H. Yu, and P. Yang, "Inversion of nighttime $PM_{2.5}$ mass concentration in Beijing based on the VIIRS day-night band," *Atmosphere*, vol. 7, 2016.

[25] D. Fu *et al.*, "Mapping nighttime $PM_{2.5}$ from VIIRS DNB using a linear mixed-effect model," *Atmos. Environ.*, vol. 178, pp. 214–222, 2018.

[26] X. Li, R. Zhang, C. Huang, and D. Li, "Detecting 2014 northern Iraq insurgency using night-time light imagery," *Int. J. Remote Sens.*, vol. 36, pp. 3446–3458, 2015.

[27] X. Li, D. Li, H. Xu, and C. Wu, "Intercalibration between DMSP/OLS and VIIRS night-time light images to evaluate city light dynamics of Syria's major human settlement during Syrian civil war," *Int. J. Remote Sens.*, vol. 38, pp. 5934–5951, 2017.

[28] M. O. Roman and E. C. Stokes, "Holidays in lights: Tracking cultural patterns in demand for energy services," *Earths Future*, vol. 3, pp. 182–205, Jun. 2015.

[29] C. C. M. Kyba *et al.*, "Artificially lit surface of earth at night increasing in radiance and extent," *Sci. Adv.*, vol. 3, Nov. 2017, Art. no. e1701528.

[30] P. Han *et al.*, "Monitoring trends in light pollution in China based on nighttime satellite imagery," *Remote Sens.*, vol. 6, pp. 5541–5558, 2014.

[31] J. Ou, X. Liu, X. Li, M. Li, and W. Li, "Evaluation of NPP-VIIRS nighttime light data for mapping global fossil fuel combustion CO_2 Emissions: A comparison with DMSP-OLS nighttime light data," *PLoS One*, vol. 10, 2015, Art. no. e0138310.

[32] T. Oda *et al.*, "On the impact of granularity of space-based urban CO_2 emissions in urban atmospheric inversions: A case study for Indianapolis, IN," *Elementa Sci. Anthropocene*, vol. 5, 2017, Art. no. 28.

[33] C. D. Elvidge, K. Baugh, M. Zhizhin, F. C. Hsu, and T. Ghosh, "VIIRS night-time lights," *Int. J. Remote Sens.*, vol. 38, pp. 5860–5879, 2017.

[34] R. J. Charlson *et al.*, "Climate forcing by anthropogenic aerosols," *Science*, vol. 255, pp. 423–430, 1992.

[35] M. Z. Jacobson, "Strong radiative heating due to the mixing state of black carbon in atmospheric aerosols," *Nature*, vol. 409, pp. 695–697, 2001.

[36] G. de Leeuw *et al.*, "Two decades of satellite observations of AOD over mainland China using ATSR-2, AATSR and MODIS/Terra: Data set evaluation and large-scale patterns," *Atmos. Chem. Phys.*, vol. 18, pp. 1573–1592, 2018.

[37] M. O. Román *et al.*, "NASA's black marble nighttime lights product suite," *Remote Sens. Environ.*, vol. 210, pp. 113–143, 2018.

[38] R.-J. Huang *et al.*, "High secondary aerosol contribution to particulate pollution during haze events in China," *Nature*, vol. 514, pp. 218–222, Oct. 9, 2014.

[39] J. Wang *et al.*, "Particulate matter pollution over China and the effects of control policies," *Sci. Total Environ.*, vol. 584–585, pp. 426–447, Apr. 15, 2017.

[40] B. Silver, C. L. Reddington, S. R. Arnold, and D. V. Spracklen, "Substantial changes in air pollution across China during 2015–2017," *Environ. Res. Lett.*, vol. 13, 2018, Art. no. 114012.

[41] J. Zhang, J. S. Reid, R. Alfaro-Contreras, and P. Xian, "Has China been exporting less particulate air pollution over the past decade?" *Geophys. Res. Lett.*, vol. 44, pp. 2941–2948, 2017.
[42] C. Song *et al.*, "Air pollution in China: Status and spatiotemporal variations," *Environ. Pollut.*, vol. 227, pp. 334–347, Aug. 2017.
[43] Y. Wu *et al.*, "On-road vehicle emissions and their control in China: A review and outlook," *Sci. Total Environ.*, vol. 574, pp. 332–349, Jan. 1, 2017.
[44] K. Baugh, F.-C. Hsu, C. D. Elvidge, and M. Zhizhin, "Nighttime lights compositing using the VIIRS day-night band: Preliminary results," in *Proc. Asia-Pacific Adv. Netw.*, 2013, vol. 35, pp. 70–86.
[45] N. Baker and H. Kilcoyne, "Joint polar satellite system (JPSS) VIIRS radiometric calibration algorithm theoretical basis document (ATBD)," Goddard Space Flight Center, Greenbelt, MA, USA, 2013.
[46] B. N. Holben *et al.*, "An emerging ground-based aerosol climatology: Aerosol optical depth from AERONET," *J. Geophys. Res., Atmos.*, vol. 106, pp. 12067–12097, 2001.
[47] D. M. Giles *et al.*, "Advancements in the aerosol robotic network (AERONET) version 3 database—Automated near-real-time quality control algorithm with improved cloud screening for sun photometer aerosol optical depth (AOD) measurements," *Atmos. Meas. Techn.*, vol. 12, pp. 169–209, 2019.
[48] K. Bessho *et al.*, "An introduction to Himawari-8/9—Japan's new-generation geostationary meteorological satellites," *J. Meteorol. Soc. Jpn., II*, vol. 94, pp. 151–183, 2016.
[49] G. Dobler *et al.*, "Dynamics of the urban lightscape," *Inf. Syst.*, vol. 54, pp. 115–126, 2015.
[50] P. Gong *et al.*, "Stable classification with limited sample: Transferring a 30-m resolution sample set collected in 2015 to mapping 10-m resolution global land cover in 2017," *Sci. Bull.*, vol. 64, pp. 370–373, 2019.
[51] X. Li *et al.*, "Anisotropic characteristic of artificial light at night—Systematic investigation with VIIRS DNB multi-temporal observations," *Remote Sens. Environ.*, vol. 233, 2019, Art. no. 111357.
[52] Z. Zhang *et al.*, "Validation of Himawari-8 aerosol optical depth retrievals over China," *Atmos. Environ.*, vol. 199, pp. 32–44, 2019.
[53] X. Cao, Y. Hu, X. Zhu, F. Shi, L. Zhuo, and J. Chen, "A simple self-adjusting model for correcting the blooming effects in DMSP-OLS nighttime light images," *Remote Sens. Environ.*, vol. 224, pp. 401–411, 2019.
[54] J. Zhang, J. S. Reid, S. D. Miller, and F. J. Turk, "Strategy for studying nocturnal aerosol optical depth using artificial lights," *Int. J. Remote Sens.*, vol. 29, pp. 4599–4613, 2008.
[55] Y.-L. Zhang and F. Cao, "Fine particulate matter (PM $_{2.5}$) in China at a city level," *Sci. Rep.*, vol. 5, Oct. 15, 2015, Art. no. 14884.
[56] N. Levin, "The impact of seasonal changes on observed nighttime brightness from 2014 to 2015 monthly VIIRS DNB composites," *Remote Sens. Environ.*, vol. 193, pp. 150–164, 2017.
[57] J. W. Marquis *et al.*, "Estimating infrared radiometric satellite sea surface temperature retrieval cold biases in the tropics due to unscreened optically thin cirrus clouds," *J. Atmos. Ocean. Technol.*, vol. 34, pp. 355–373, 2017.
[58] D. M. Winker *et al.*, "Overview of the CALIPSO mission and CALIOP data processing algorithms," *J. Atmos. Ocean. Technol.*, vol. 26, pp. 2310–2323, 2009.
[59] Á. Barreto *et al.*, "The new sun-sky-lunar Cimel CE318-T multiband photometer—A comprehensive performance evaluation," *Atmos. Meas. Techn.*, vol. 9, pp. 631–654, 2016.

Xuejun Wang Xuejun Wang received the B.E. degree in environmental engineering from the University of Electronic Science and Technology of China, Chengdu, China, in 2016. She is currently working toward the Ph.D. degree in cartography and geographic information system with Faculty of Geographical Science, Beijing Normal University, Beijing, China.

Her current research interests include the retrieval of atmospheric parameters from satellite data and the application of nighttime light satellite data.

Xihan Mu received the B.S. degree in computer science and technology from the College of Information Science and Technology and the Ph.D. degree in remote sensing from the School of Geography, Beijing Normal University, in 1999 and 2009, respectively.

He was a visiting student with the Laboratoire des Sciences de l'Images, de l'Informatique et de la Télédétection, Louis Pasteur University, in 2007, and a Visiting Scientist with the Commonwealth Scientific and Industrial Research Organisation in 2016. He is currently with the Faculty of Geographical Science, State Key Laboratory of Remote Sensing Science, Institute of Remote Sensing Science and Engineering, Beijing Normal University, Beijing. His research interests focus on multiangular remote sensing, particularly in the retrieval/measurement of vegetation structural parameters.

Guangjian Yan (Senior Member, IEEE) received the Ph.D. degree in cartography and geographic information system from the Institute of Remote Sensing Applications, Chinese Academy of Sciences, Beijing, China, in 1999.

He is currently a Professor with the State Key Laboratory of Remote Sensing Science, Institute of Remote Sensing Science and Engineering, Faculty of Geographical Science, Beijing Normal University, Beijing, China. He has authored or co-authored more than 160 papers. His main research interests are multiangular remote sensing, vegetation remote sensing, radiation budget, scale effect, and scale correction of remote sensing.